



OPEN ACCESS

EDITED BY
Ahmed U. Abdelhady,
Verisk Analytics, United States

REVIEWED BY
Luping Yang,
University of California, Berkeley,
United States
Changda Feng,
Florida International University,
United States
Daniel Rhee,
University of Illinois at Urbana-
Champaign, United States

*CORRESPONDENCE
Christian Bedwell,
cabedwell@ufl.edu

SPECIALTY SECTION
This article was submitted to Wind
Engineering and Science,
a section of the journal
Frontiers in Built Environment

RECEIVED 12 August 2022
ACCEPTED 19 October 2022
PUBLISHED 02 November 2022

CITATION
Bedwell C, Gurley K, Pinelli J-P and
Silva de Abreu RV (2022), The influence
of ASCE 7–16 wind load provisions on a
vulnerability model of Florida
residential construction.
Front. Built Environ. 8:1018207.
doi: 10.3389/fbuilt.2022.1018207

COPYRIGHT
© 2022 Bedwell, Gurley, Pinelli and Silva
de Abreu. This is an open-access article
distributed under the terms of the
[Creative Commons Attribution License
\(CC BY\)](#). The use, distribution or
reproduction in other forums is
permitted, provided the original
author(s) and the copyright owner(s) are
credited and that the original
publication in this journal is cited, in
accordance with accepted academic
practice. No use, distribution or
reproduction is permitted which does
not comply with these terms.

The influence of ASCE 7–16 wind load provisions on a vulnerability model of Florida residential construction

Christian Bedwell^{1*}, Kurtis Gurley¹, Jean-Paul Pinelli² and Roberto Vicente Silva de Abreu²

¹Department of Civil and Coastal Engineering, University of Florida, Gainesville, FL, United States,

²Department of Mechanical and Civil Engineering, Florida Institute of Technology, Melbourne, FL, United States

The Florida Public Hurricane Loss Model is a probabilistic risk model designed to estimate wind induced insurance losses to residential infrastructure in Florida. In the physical damage estimation module, Monte Carlo simulation is employed to generate damage matrices as a function of wind speed by comparing probabilistic building component capacities to wind loads. These damage matrices are input to a repair cost algorithm, ultimately producing damage ratios as a function of wind speed for different building classes. It is required that the inventory of residential building models reflect the history of construction practice within Florida. Differing eras of construction are represented by developing component-wise options for probabilistic capacities and load paths, resulting in a suite of hundreds of model variants. Regarding loads, the probabilistic wind load model is based on a directionalized adaptation of ASCE 7, and its representation in the model is kept current with the version adopted by the Florida Building Code (FBC). In 2020 the Florida Building Code adopted by reference ASCE 7–16, which contains important changes to the wind-load provisions. These changes have implications for both the loading and resistance aspects of the physical damage model, thus influencing insured loss projections. This study discusses the development and implementation of these changes within the model and investigates the impacts on the modeled vulnerability of residential structures in Florida. Comparing vulnerability estimates of structures designed before and after the FBC adoption of ASCE 7–16 provide insight into the potential effectiveness of such changes to improve community resilience.

KEYWORDS

hurricane, wind, risk modeling, vulnerability, building codes

1 Introduction

Early models of infrastructure vulnerability to hurricane hazards were based on relationships between historical insurance loss data and local recorded wind speeds (Friedman, 1975; SWFRPC, 1982; Berke et al., 1984; Ruch, 1984). Studies performed at Clemson University integrated engineering knowledge into hurricane vulnerability models; a threshold wind speed was defined which represented significant damage to the building envelope to allow water intrusion (Sparks and Bhinderwala, 1994). Simulation models, which first appeared in the late-1990s, developed more engineering-grounded relationships between building damage and wind speed (Sciaudone et al., 1997). The Federal Emergency Management Agency and National Institute of Building Safety developed HAZUS, a methodology designed to estimate risk due to a wide variety of natural hazards (FEMA-HAZUS, 2006). Since the widespread adoption of simulation-based hurricane hazard models, many advances have been made to estimate damage. Methodologies have been developed to model the effects of progressive damage to the building envelope over the course of a wind event (Ji et al., 2020), to use a network of simulations to model the time-history of a wind event and several structures' responses (Lin et al., 2019), and concurrently model the impacts of wind, surge, and wave hazards at a regional scale (Nofal et al., 2021). A comprehensive review of hurricane vulnerability estimation methods can be found in Pita et al., 2014, while the most recent contribution in the context of residential construction can be found in Abdelhady et al., 2022.

The Florida Public Hurricane Loss Model (FPHLM) is a probabilistic risk model designed to produce estimates of insured losses caused by hurricane wind-induced damage to residential structures within the state of Florida. The methods and outputs from this State of Florida funded risk model are evaluated and certified on a biennial basis by the Florida Commission on Hurricane Loss Projection Methodology (Florida International University, 2021). During this evaluation it must be demonstrated that the model employs the current state of knowledge in wind hazard science, incorporates assumptions that reflect historical and current building practice in Florida, and accurately simulates wind-induced physical damage and vulnerability. Herein we define vulnerability as the monetary damage ratio, which is the ratio of the cost of repair to building value.

The FPHLM began development in 2002 and was first certified by the Florida Commission on Hurricane Loss Projection Methodology in 2007. The model has been continually refined and updated to keep pace with the current state of knowledge, new datasets from wind events, and changes in the aspects of codes and standards that influence wind vulnerability. While not inclusive of all available FPHLM peer reviewed documentation, the following review provides sufficient background for the engineering components and validation of the model. Insurance portfolios from three major storms were

compared with predicted losses in a validation study (Pinelli et al., 2008). An overview of major model components was written and sample probable maximum loss outputs for 30 hypothetical Florida landfalling storms were produced (Hamid et al., 2010; Hamid et al., 2011). The FPHLM simulates the co-occurrence of wind, rain, and envelope damage to estimate interior damage (Pita et al., 2012). Experimental test results on wind-driven rain intrusion into residential structures (Baheru, 2014) were used to further refine the FPHLM interior damage model (Johnson et al., 2018). Later tests performed at the Florida International University's Wall of Wind provided insight into the physical mechanisms of rainwater ingress. The results of these tests were used to develop a more thoroughly defined model of interior damage, which accounts for the propagation and distribution of water throughout various components in the structure (Silva de Abreu et al., 2020). Beyond the direct application of producing estimated losses, the FPHLM has also been utilized to evaluate the effectiveness of various mitigation techniques. Models with combinations of mitigated components (e.g. shuttered windows, roof retrofit devices, gable-end bracing) were used in a cost-benefit analysis to evaluate the effectiveness of mitigation techniques based on region and structure type (Torkian et al., 2014).

The Florida Building Code (FBC) seventh Ed., effective as of December 2020, adopts by reference the ASCE 7-16 standard to calculate design wind loads (International Code Council, 2020). Relative to its predecessor ASCE 7-10, the ASCE 7-16 standard contains significant changes to the calculation of uplift loads on roof components and cladding. In both versions of ASCE 7, the roof system is divided into zones with varying uplift load coefficients. In ASCE 7-16, these zones were redefined, and changes to the load coefficients result in an increased uplift load on roof components and cladding (American Society of Civil Engineers, 2017). These changes to roof loading (described in detail in Section 3.1), present two tasks for the FPHLM modelling team to keep the model in compliance with current knowledge and construction practice. First, the modified roof loading reflects the current understanding of wind-induced loads and should be integrated into the FPHLM's wind loading algorithm. Second, the FBC has updated construction requirements (building code changes) in response to these new design wind loads upon adoption of ASCE 7-16. Florida residential structures built to the FBC seventh Ed. will comprise a non-negligible portion of the inventory as time passes. As the FPHLM includes structural models from various eras in residential building code history, the notable changes to the FBC call for a new model to represent post-2020 construction.

This paper describes the development and implementation of the above two tasks. The resultant loading and construction changes to the model are analyzed in isolation and in combination to understand the influence each modification has on the vulnerability outputs of the FPHLM.

2 The Florida Public Hurricane Loss Model (FPHLM)

The FPHLM consists of three components: a meteorological (hazard) module, a vulnerability (engineering) module, and an actuarial module. The meteorological module produces the peak wind speeds at 10 m height for actual terrain, at any location in Florida, for each of the 50,000 + simulated hurricanes of a stochastic set. The vulnerability module produces vulnerability matrices describing the relationship between wind speed and damage ratio. These matrices are produced for a library of different models reflecting the construction eras that make up the current Florida residential inventory. Separate vulnerability matrices are produced for physical building, appurtenant structures, interior contents, and additional living expenses. The actuarial module uses the outputs from the vulnerability and meteorological modules to produce, for example, average annual insured losses for any given portfolio of properties, or region of Florida, or era of construction, *etc.*

Changes to the Florida Building Code resulting from the adoption of ASCE 7–16 have a direct impact on the vulnerability module. Comprehensive documentation of the FPHLM, including flow charts for the full system and individual modules are publicly available (Florida International University, 2021). The modifications discussed in this paper are confined to the model that represents timber frame construction and gable roof shapes. Parallel modifications to models that reflect masonry wall structures and hip roof shapes are omitted for brevity.

2.1 Physical damage estimation component

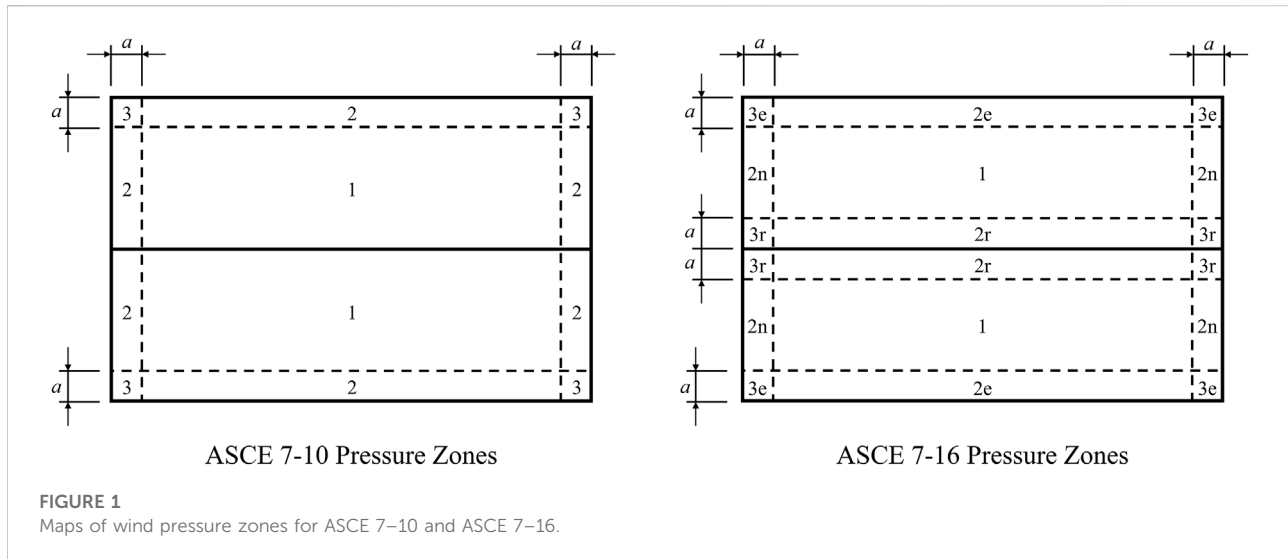
The damage estimation component of the vulnerability module of the FPHLM simulates wind-induced damage to the structural components of model buildings. Monte Carlo simulation is utilized to capture uncertainties in many aspects of the load to damage chain. For a given model type (e.g. single story timber frame gable roof constructed in 1983), many simulations are conducted for a sequence of wind speeds and wind directions. Each simulation consists of a randomized representation of wind loading and component capacities. The specific probability distributions used for the randomization are dependent on building type, shape, age, and wind direction. Deterministic relationships define load paths, load sharing, and the influence of damaged components on building loads. For example, a broken window changes internal pressure and therefore net loads on roof sheathing, walls, and other windows. The outcome of a given simulation is a single sample of how many of each modeled building component fails (load exceeds capacity). The next simulation ‘rebuilds’ the same model with a fresh randomized representation of wind

TABLE 1 Components evaluated for damage.

| Column | Value description |
|--------|--|
| 1 | Percentage of failed roof sheathing |
| 2 | Percentage of lost roof cover |
| 3 | Percentage of failed roof-to-wall connections |
| 4 | Number of failed walls |
| 5 | Number of failed windows |
| 6 | Number of failed doors |
| 7 | Number of failed garage doors |
| 8 | Binary indicator for building breach (1 if window/door/garage door was damaged, 0 otherwise) |
| 9 | Total number of windows broken by missile impact |
| 10 | Percentage of failed gable-end panels (zero if hip roof) |
| 11 | Calculated internal pressure |
| 12 | Percentage of failed wall sheathing panels (front wall) |
| 13 | Percentage of failed wall sheathing panels (back wall) |
| 14 | Percentage of failed wall sheathing panels (side wall) |
| 15 | Percentage of failed wall sheathing panels (side wall) |

loading and component capacities for the same wind speed and wind direction. This continues through all assigned wind speeds and wind directions, producing a 4-dimensional ‘damage matrix’ where each row is the outcome of a simulation, each column is a building component (Table 1), the third dimension is 3-s gust wind speed, and the fourth dimension is wind direction. Each cell in any given row of the 4-D damage matrix expresses the quantity of damage to each component at each wind speed and each wind direction for one simulation. Averaging this 4-D damage matrix over all simulations and all wind directions produces a quantification of average damage to each modeled building component as a function of wind speed. The default wind speeds are 50–250 mph 3-s gust in five mph increments. The default wind directions are eight approach angles in 45° increments. For each combination of wind speed and approach angle, 2,000 simulations are performed. This represents $41 \times 8 \times 2,000 = 656,000$ simulations in each completed damage matrix.

The same Monte Carlo engine would be used if the subject were a masonry wall hip roof building built in 2019. However, the probability distributions used for randomized building component capacities are different (material and building code differences), some aspects of load sharing are different, the wind loading scheme is different (hip and gable roof shapes load differently), and therefore the contents of the resultant damage matrix would be quite different from the 1983 built timber frame gable roof building. For that reason, many model variants were developed to represent the vast Florida inventory. Model variants include different building materials, roof shapes, eras of construction, common maintenance practices (e.g., an old structure with new roof shingles), mitigation measures (e.g., window protection against debris), and regions with specific



design requirements (e.g., windborne debris region requirement for window protection).

The influence of a change to any component of a physical damage model can be investigated by implementing that change, using simulation to generate a damage matrix with and without that change, and plotting the before and after versions of the mean component damage vs. wind speed. In some cases, changing the capacity of one component may change the damage to other components, so plotting each component before and after is valuable. For example, comparing the damage with and without the use of window protection will reveal changes in mean damage to windows, roof sheathing and walls. However, this process does not provide quantitative insight with respect to changes in projected monetary damage. Will the use of window protection reduce predicted annualized average damage by \$5 or \$5000? For that obviously relevant insight, the physical damages must be converted to cost of repair.

2.2 Interior damage and vulnerability components

The 4-D damage matrix describing physical damage to the building's external components in [Table 1](#) is the input to the next process in the vulnerability module, the interior damage component. For each simulation, this component predicts interior damage to the building due to rain-water ingress through both damaged components (windows, roof cover and sheathing) and rain-water pathways through undamaged components (e.g., gaps in the window-wall interface under large pressure loads).

The final component of the vulnerability module converts the combined physical external and interior damage into monetary damage and generates damage ratios of total cost of repair over the value of the building. For each structure, these damage ratios

are used to generate a vulnerability matrix. In these vulnerability matrices, each column represents the mean 3-s gust wind speed, and each row corresponds to a range of damage ratios. The value of each cell is the conditional probability of a damage ratio occurring at a given wind speed. A building vulnerability matrix can be represented graphically as a vulnerability curve, the plot of the mean damage ratio vs wind speed. Although the FPHLM uses the matrix and not the curve to compute losses, the curve provides a visual interpretation of the influence of all building component repair costs. Changes and/or updates to the components of the physical damage models can now be evaluated within the framework of how they influence the building vulnerability curve. This provides the \$5 vs. \$5000 insight desired at the end of the previous section. These vulnerability curves will be the basis for investigating the changes to the FPHLM as a result of the FBC adoption of ASCE 7–16. Examples are shown in [Section 5](#).

This paper uses vulnerability matrices and curves derived from building damage ratios, which describe the cost of repairs to the external and internal components of the structure. Additionally, the vulnerability module also produces matrices for contents damage, damage to appurtenant structures, and additional living expenses. Vulnerability matrices can also be developed for interior damage, excluding the damage to external structures.

3 Code change description and implementation in FPHLM

3.1 Relevant code changes

A comprehensive survey of the changes from FBC sixth Ed. to FBC seventh Ed. was conducted to identify modifications that

were relevant to structural wind resistance. This survey was accompanied by a literature review of materials written to highlight and explain relevant code changes (Chock et al., 2018; Scott, 2018; Building a Safer Florida, 2020a; Building a Safer Florida, 2020b; Florida Building Commission, 2020).

ASCE 7–16, Chapter 30 defines the method by which wind loads are calculated on the components and cladding (C&C) of structures. A notable change between ASCE 7–10 and ASCE 7–16 involves specific details within the uplift load calculations on roof C&C. The underlying mechanical principles remain the same: the net pressure on a component is calculated using

$$p = q_h \cdot (GC_p - GC_{pi}) \quad (1)$$

where p is the design wind pressure (psf), q_h is the velocity pressure (psf), GC_p is the external pressure coefficient, and GC_{pi} is the internal pressure coefficient. The velocity pressure, q_h , is defined by

$$q_h = 0.00256 \cdot K_h \cdot K_{zt} \cdot K_d \cdot K_e \cdot V^2 \quad (2)$$

where K_h is the velocity pressure exposure coefficient (equal to 0.85), K_{zt} is the unitless topographic factor (assigned to unity), and V is the wind speed (mph). The directionality coefficient, K_d , is set to unity in our application because the FPHLM damage model explicitly considers multiple directions. The ground elevation factor, K_e , which accounts for the change in air density at various elevations, is set to its sea level value given the typical ground elevation in Florida. The highest elevation in Florida is 345 feet above sea level (WJHG News, 2017).

The relevant change between ASCE 7–10 and ASCE 7–16 concerns both the magnitude and mapping of the external pressure coefficient, GC_p , to the roof surface. Chapter 30 of ASCE seven includes a series of maps and plots for hip and gable roof shapes. The maps delineate pressure zones, and accompanying plots define GC_p in each of those zones as a function of effective wind area. The ASCE 7–16 pressure zone map for gable-roof structures makes a distinction between the previously-united zones 2e and 2n, and includes the new zones 2r and 3r along the ridge line (Figure 1). The plot defining the pressure coefficients in each zone changed significantly from ASCE 7–10 to 7–16; the plot not only accounts for new zones, but also significantly increase the GC_p across most regions of the roof at most effective wind areas (ASCE, 2013; ASCE, 2017). In summary, the C&C roof uplift design pressure coefficients increased from 7 to 10 to 7–16.

The increase in the external pressure coefficient led to a notable change in the FBC seventh Ed concerning roof sheathing fasteners. FBC Section R803.2.3.1 governs allowable roof sheathing fastener types and spacing. Design wind speed, specific gravity of the roof sheathing, and truss/rafter spacing are all factors that influence allowable fastener design in both sixth Ed. and seventh Ed. Under FBC seventh Ed., both the type and spacing requirements became stricter. RSRS-01 ring-shank

nails are required in FBC seventh Ed., whereas 8 days nails, which have a weaker withdrawal capacity (Skulteti et al., 1997; Prevatt et al., 2009), were allowable in many structures under the FBC sixth Ed. Regarding fastener spacing, 12-inch spacing between fasteners was allowed at design wind speeds less than or equal to 140 mph under FBC sixth Ed. Under FBC seventh Ed., 12-inch fastener spacing is only allowed for certain structures at design wind speeds of 120 mph or less (International Code Council, 2017; International Code Council, 2020).

3.2 Changes to FPHLM loading

The new wind load provisions in ASCE 7–16 require a change to the C&C loading scheme in the FPHLM. The previous versions of the FPHLM developed modifications to the ASCE 7–98 directionally enveloped pressure maps to explicitly model eight approach wind angles (Cope, 2004). The FPHLM maps were developed for winds parallel to the ridge line, winds perpendicular to the ridge line, and cornering winds. For the current FPHLM modification, a similar approach was utilized to develop the directionalized pressure zone maps based on ASCE 7–16 (Figure 2).

For each sheathing panel, the uplift load is calculated as a uniform pressure using Eq. 1, where GC_p is the weighted average of pressure coefficients overlapping that panel according to the relevant directionalized wind pressure zone map. Table 2 provides a summary of all values of GC_p used in the gable-roof model prior to and after the adoption of ASCE 7–16.

Although only the pressure coefficients for zones 1 and 3r increase from ASCE 7–10 to ASCE 7–16, the total modeled uplift load across the roof increases. Considering Eq. 1, since the design wind pressure q_h is uniform, the weighted average of external pressure coefficients across the roof can be used as a proxy for the total uplift load. The average GC_p for each approach angle under each loading scheme was calculated (Table 3). Averaging across all approach angles (noting that cornering winds account for four out of eight approach angles) results in an average GC_p increase from -1.166 to -1.416 . This change accounts for a 21.4% increase in uplift load from ASCE 7–10 to ASCE 7–16 as the concept is manifested within the FPHLM.

3.3 Changes to FPHLM building models

Residential structures designed under ASCE 7–16 require higher capacity components to resist the increased uplift loads. In the FPHLM, this is reflected in the development of a new variant of the current ‘strong’ model that represents pre-seventh Edition FBC construction outside of Miami/Dade and Broward Counties in Florida (outside of the high velocity hurricane zone - HVHZ). This new strong variant that represents ASCE 7–16 design wind loads is referred to as the new strong model.

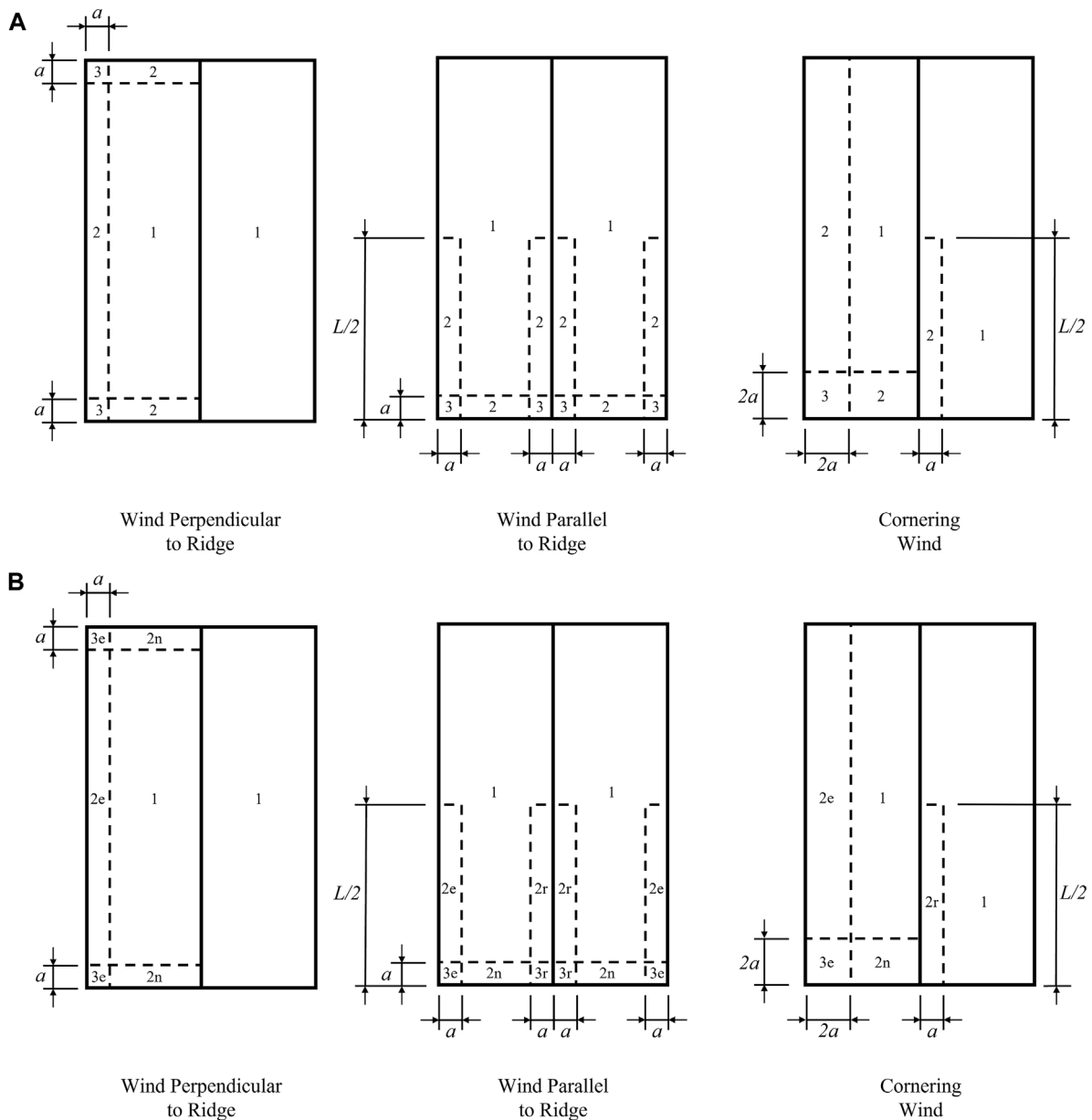


FIGURE 2 Modified wind pressure zone maps for (A) ASCE 7–10 and (B) ASCE 7–16.

In the FPHLM, the uplift load path is comprised of roof sheathing, roof-to-wall connections, and stud-to-sill connections. In the strong model, the sill to foundation is not explicitly modeled and sufficient capacity is presumed. Uplift pressures are calculated as a uniform pressure on any given roof sheathing panel as a weighted sum of that panel’s overlay within one or more pressure zones. Each sheathing panel is then evaluated for damage triggered by pressure exceeding uplift capacity, which has been randomly assigned as a function of sheathing fastener type and spacing. The uplift pressure applied to all non-damaged roof sheathing panels is then

TABLE 2 External pressure coefficients in FPHLM.

| Zone | GC_p (ASCE 7–10) | GC_p (ASCE 7–16) |
|------|--------------------|--------------------|
| 1 | -0.9 | -1.38 |
| 2e | -2.1 | -1.38 |
| 2n | -2.1 | -1.94 |
| 2r | -2.1 | -1.38 |
| 3e | -2.1 | -1.94 |
| 3r | -2.1 | -2.12 |

TABLE 3 Average GC_p across roof using modified pressure zone maps.

| Approach angle | Average GC_p (ASCE 7–10) | Average GC_p (ASCE 7–16) |
|-----------------------------|----------------------------|----------------------------|
| Wind Perpendicular to Ridge | -1.067 | -1.415 |
| Wind Parallel to Ridge | -1.163 | -1.415 |
| Cornering Wind | -1.217 | -1.417 |

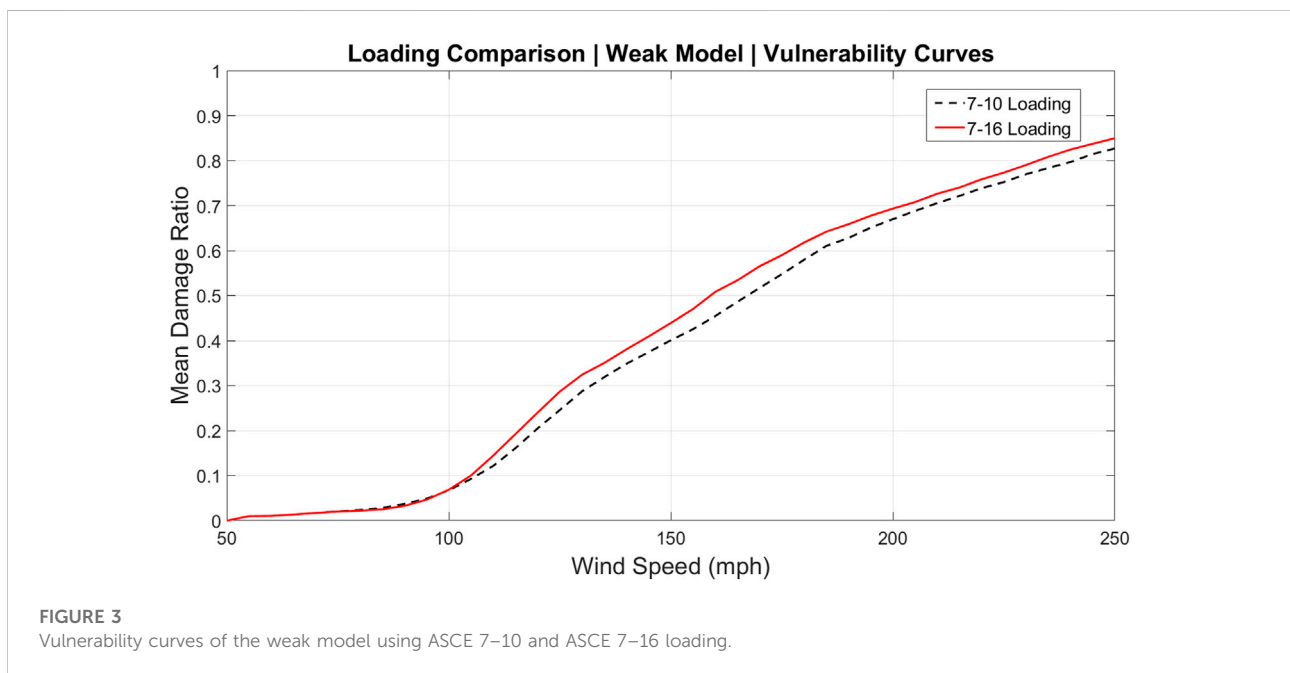
TABLE 4 Summary of component changes in new strong model.

| Component | Strong model capacity | New strong model capacity |
|-------------------------|-----------------------|---------------------------|
| Sheathing fastener | 130 psf | 200 psf |
| Roof-to-wall connection | 3,720 lb | 6,750 lb |
| Stud-to-sill connection | 2023.5 lb/ft | 3,000 lb/ft |

Ed., the new strong model uses ring-shank nails at 6/6 spacing. This change results in an increase in the mean uplift capacity of sheathing panels from 130 psf to 200 psf (Prevatt et al., 2009).

The increase in uplift loads results in larger loads at the roof-to-wall connections. The modelers utilized design capacities and factors of safety from Simpson Strong-Tie to assign the capacity of roof-to-wall connections and stud-to-sill connections (Strong-Tie Company, 2021). For roof-to-wall connections, the new strong model capacity has been upgraded with higher capacity tiedowns, resulting in an increase in the mean uplift capacity from 3,720 lb to 6,750 lb. Likewise, upgrades to the stud-to-sill connections result in a mean capacity increase from 2023.5 lb/ft to 3,000 lb/ft. The changes from the strong model to the new strong model are summarized in Table 4.

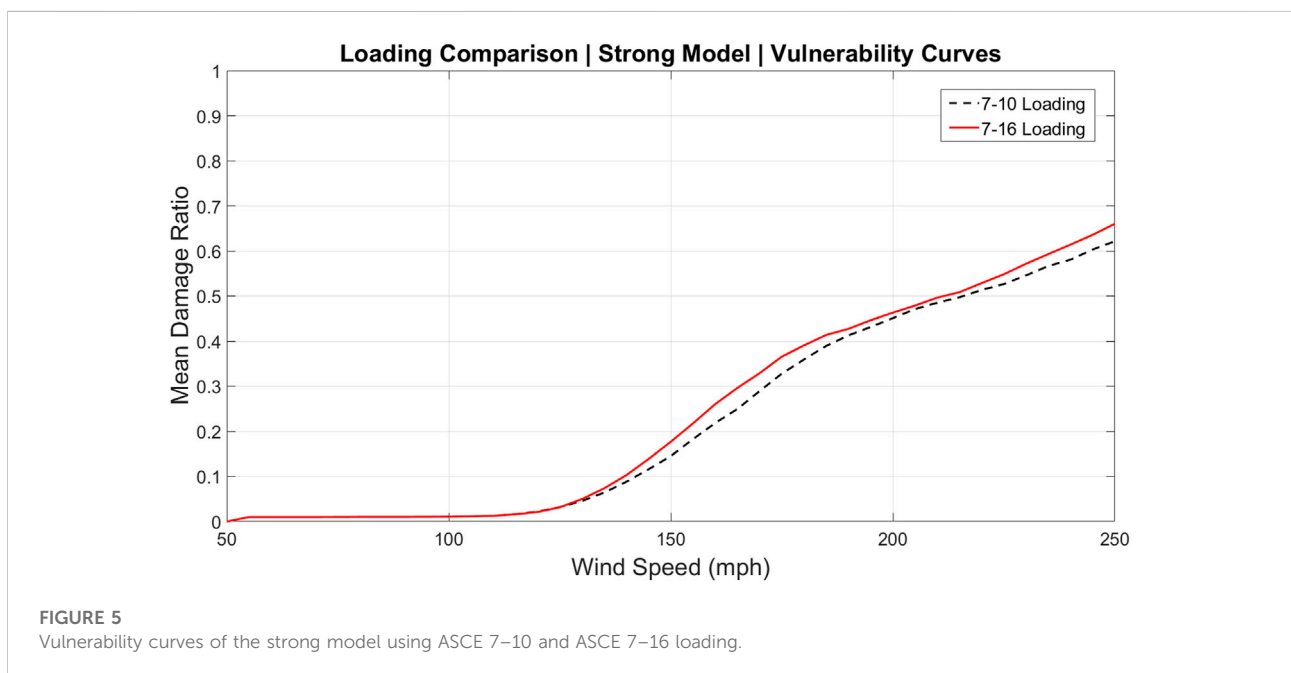
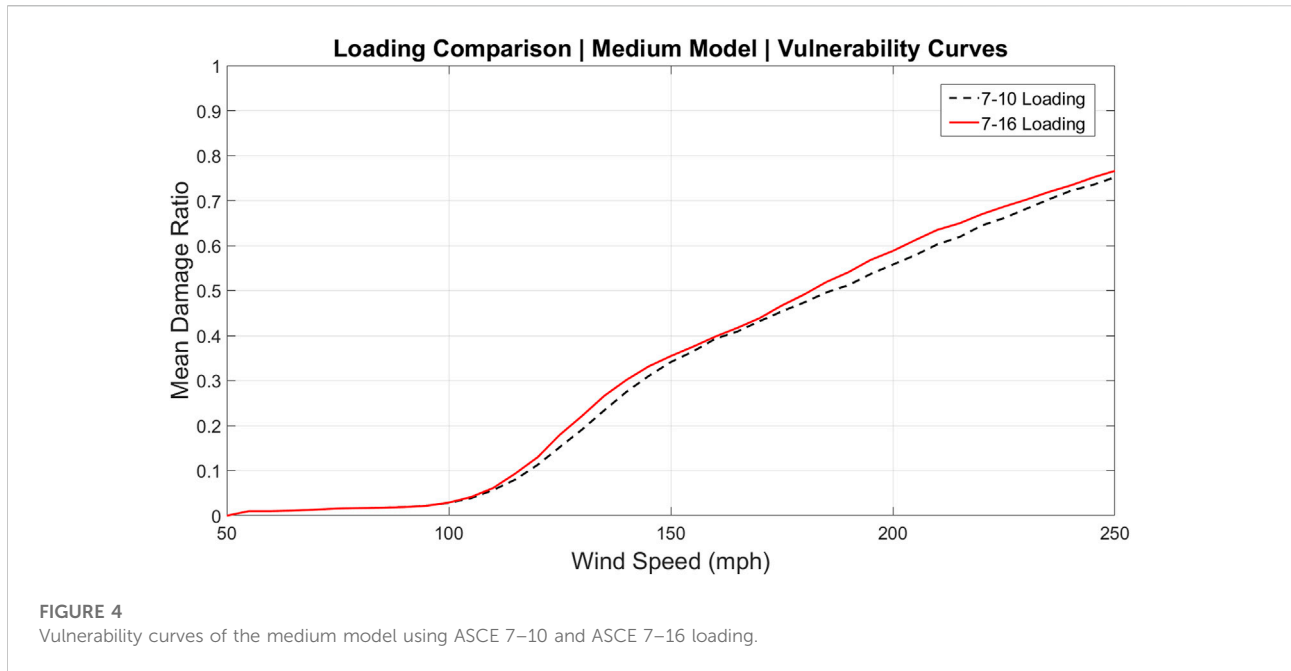
The method of assigning random component capacities is described for the components under discussion. For each roof sheathing panel, a random value is assigned from a truncated normal distribution with a coefficient of variation (COV) of



redistributed to the roof-to-wall connections. After these connections are evaluated for damage, the uplift load in each connection is transferred to the wall. The wall is evaluated for damage with a combination loading limit state, combining the effects of uplift, bending, and shear loading.

The strong model utilizes 8 days nails for roof sheathing fasteners using 6/6 spacing (nails are spaced 6 inches apart on center along panel edges, and along intermediate supports within the panel field). In compliance with Section R803.2.3.1 of FBC seventh

0.25 for weak and medium models, and 0.20 for strong and new strong models. The truncation limits values to within 2 standard deviations of the mean capacity. For stud-to-sill connections the uplift capacity is selected from a truncated normal distribution using a COV of 0.2. For roof to wall connections the weak model represents toe nail connections with a truncated normal distribution and a COV of 0.2. The medium, strong, and new strong variations use a COV of 0.05 to represent the low variability among these highly engineered and consistent roof-to-wall connection products.

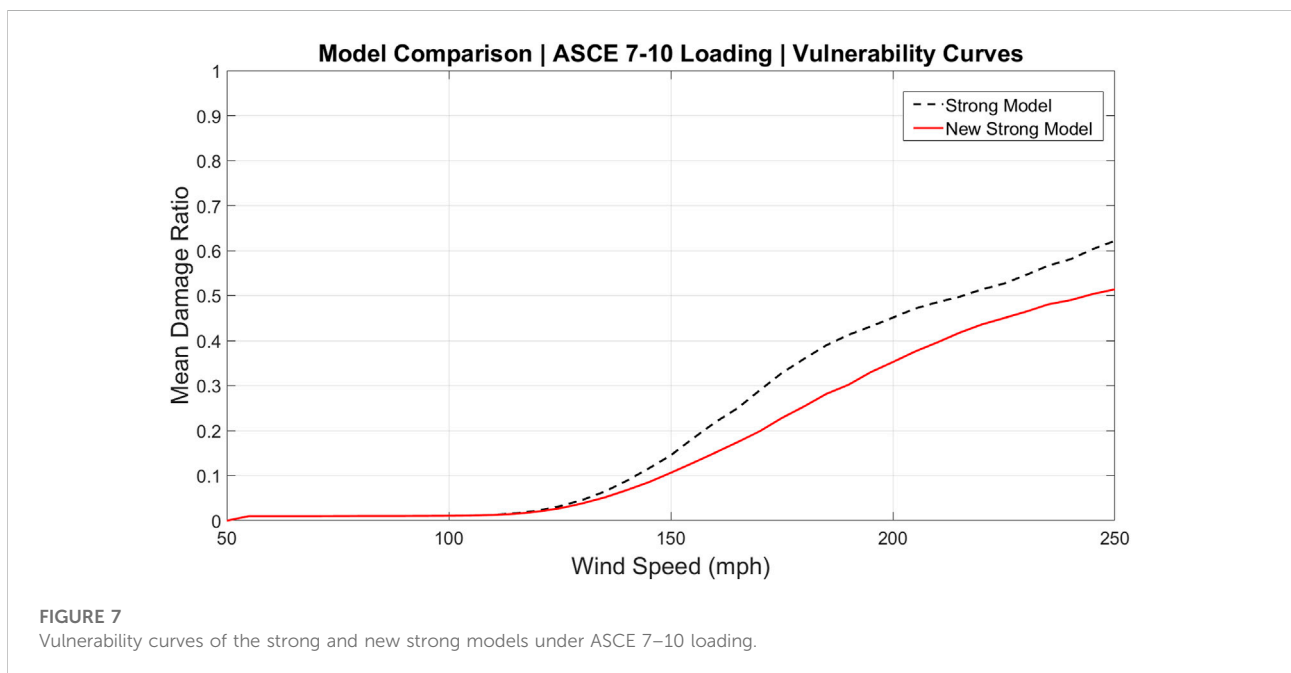
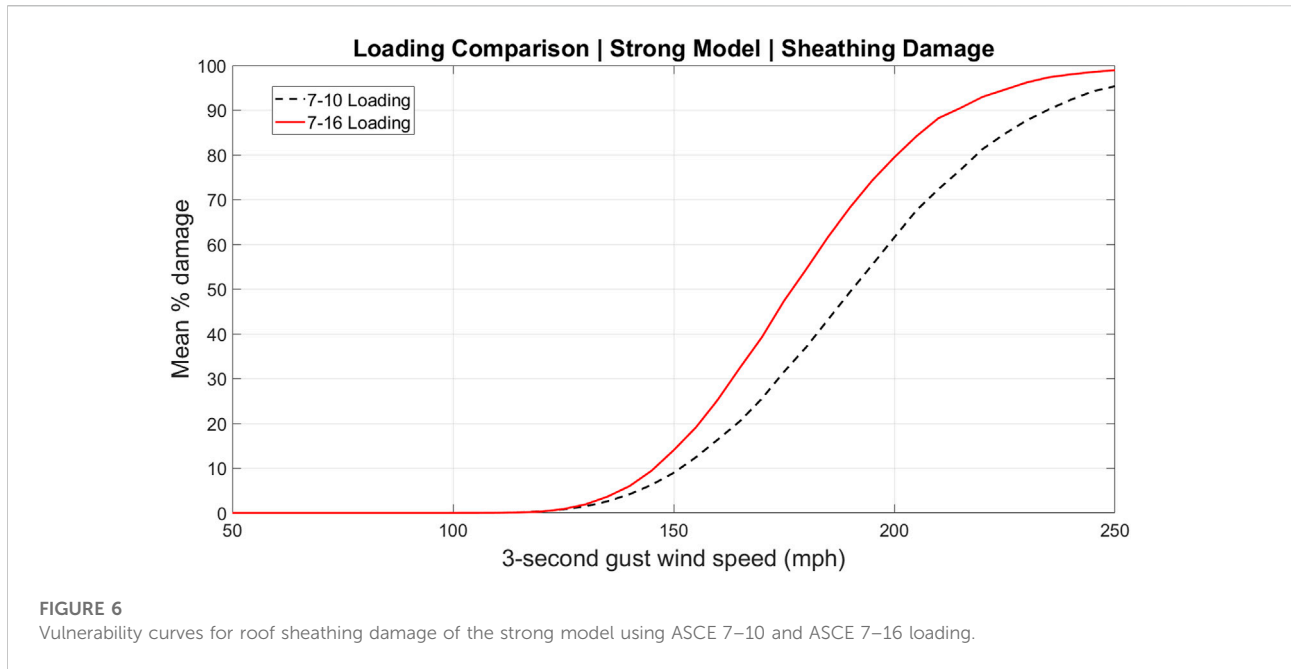


4 Methodology

The new strong model was developed by implementing changes to both the directionalized roof uplift loading scheme and the mean capacities of structural components in the uplift load path, as described in the previous sections. The influence of

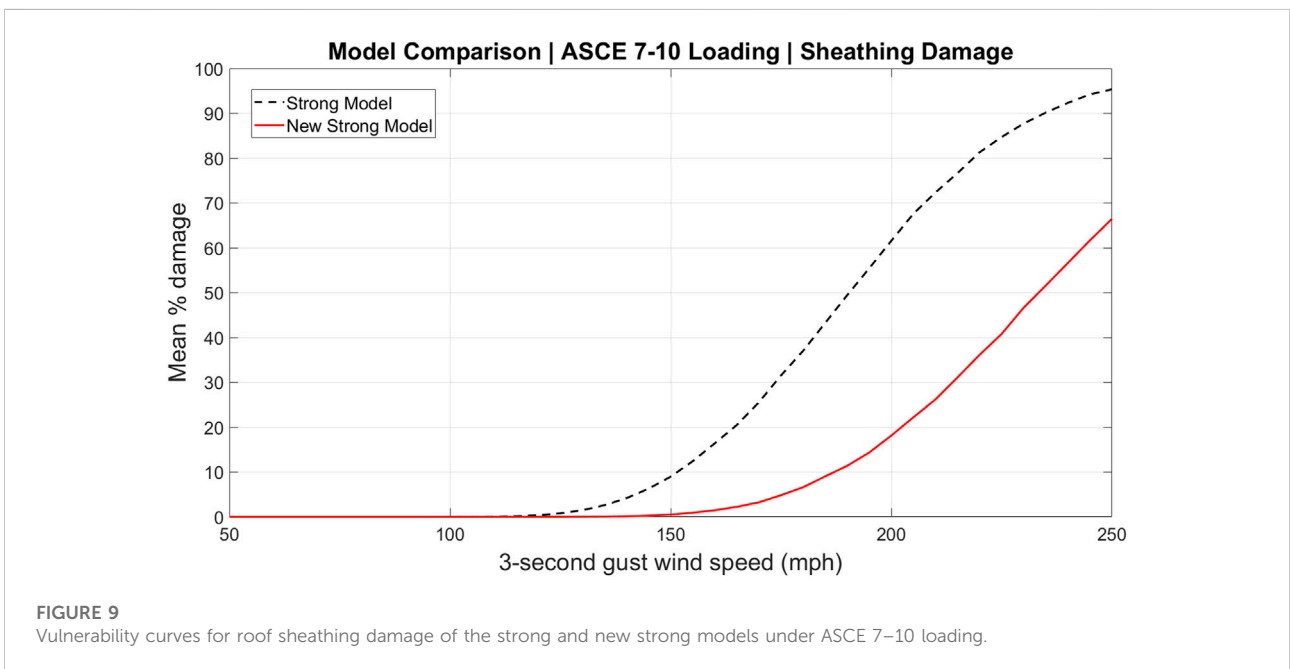
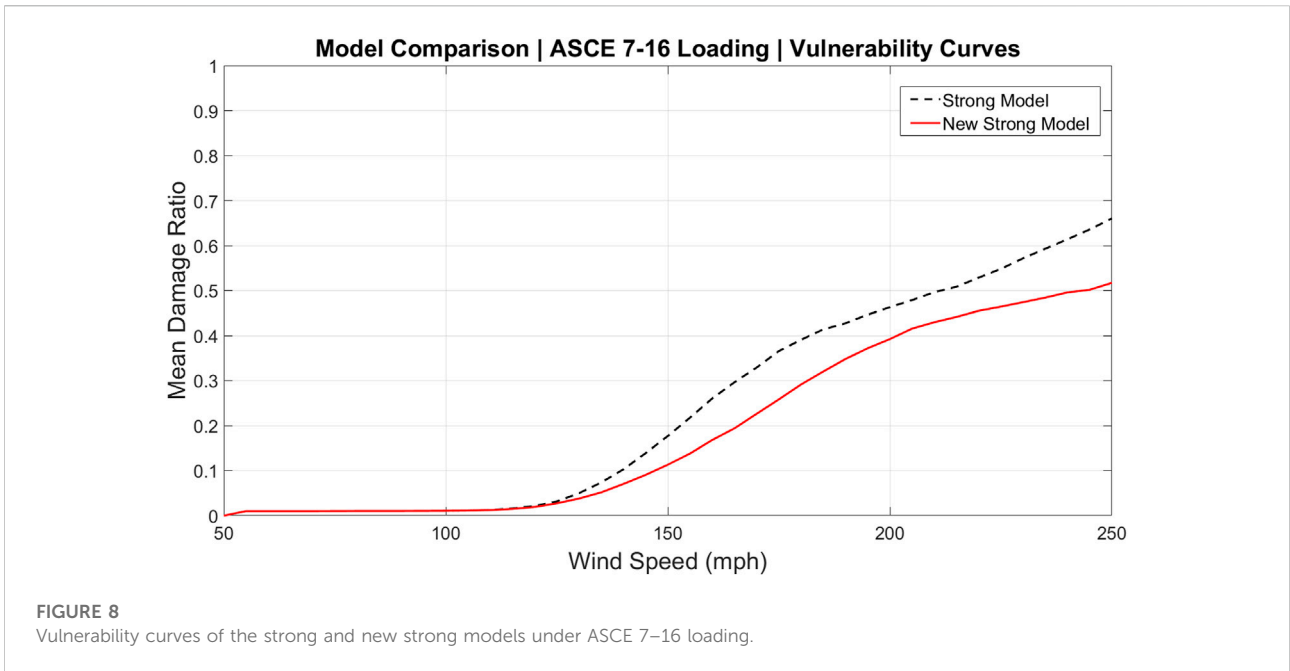
these independent changes to load and capacity on model outputs is investigated separately and in combination.

The influence of changes to the roof uplift loading scheme is evaluated on a subset of the existing library of models. Recall that many variants of the structural model have been developed to reflect different eras of construction



as well as mitigation and maintenance. The base models include weak, medium and strong versions. The strong version represents post-1994 construction after significant changes to building methods and state level enforcement as a result of Hurricane Andrew. The weak model broadly represents construction before wind resistant features were commonly used in construction, such as toe nailed roof-to-

wall connections prior to the common use of clips (medium model) or straps (strong model). Many subvariants of each base model were also developed (base weak but with new roof cover and re-nailed decking, all models with and without window protection, etc.). Herein, the influence of changes to wind loading on model outputs is confined to the base weak, medium, and strong models of the timber-frame gable-roof

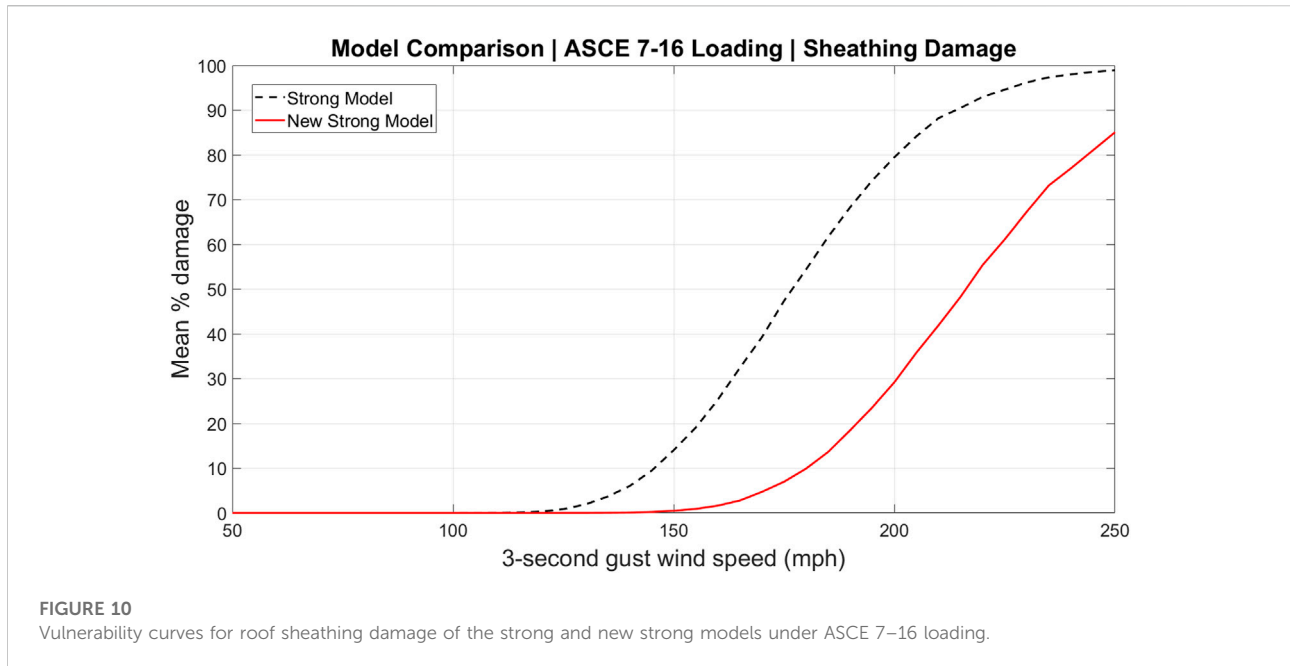


structure. For each of these models, physical damage matrices were generated *via* Monte Carlo simulation and input to the vulnerability model to generate internal damage and then vulnerability curves. Similarly, the influence of changes to component capacities is evaluated by comparing the base strong model and the new strong model under both ASCE 7–10 (previous) and ASCE 7–16 (new) loading schemes.

5 Analysis

5.1 Effects of new wind-loading calculations

Each vulnerability curve (Figures 3–5, Figures 7, 8), presents the mean damage ratio (ratio of repair cost to building value) as a function of the 3-s gust wind speed.



Figures 3–5 each contain vulnerability curves of the identical building model (weak, medium and strong, respectively), as exposed to ASCE 7–10 and ASCE 7–16 loading. In each figure, the vulnerability curves being compared are nearly identical before 100 mph and then separate when exterior component damage starts to accumulate, and the influence of the different load schemes becomes visible. This separation occurs at increasing wind speed from weak to medium to strong models, reflecting less vulnerability to damage for better construction quality. After this separation, each model experiences greater damage under ASCE 7–16 loading. This outcome aligns with expectations, as the new loading scheme produces higher uplift loads and therefore more roof cover and sheathing damage, and more water penetration through the damaged roof.

Figures 3–5 model results for two loading schemes encompasses the influence of all modeled building components. The vulnerability of individual components can also be isolated as in Figure 6 which presents mean percent damage to the strong model roof sheathing panels using both loading schemes. The relative influence of the many individual components to overall vulnerability was investigated previously for the FPHLM (Torkian et al., 2014).

5.2 Effects of increased component capacities

Figures 7, 8 each contain vulnerability curves for the strong model and new strong model. Figure 7 compares these

models under ASCE 7–10 loading; Figure 8 uses the newly implemented ASCE 7–16 loading. Under both loading schemes, the strong model is more vulnerable than the new strong model. These figures reveal that the mean capacity changes have a stronger influence on the damage ratio than the loading changes. In most cases, the changes due to loading led to differences in vulnerability of less than 5% (Figures 3–5). However, the assigned changes to the capacity of the components in the new strong model result in a decrease in vulnerability by well more than 5% (Figures 7, 8). The result is that the simultaneous application of the new loading scheme and new strong model capacities produce a damage curve (Figure 8 red solid curve) that is less vulnerable than the pre-2020 FBC strong model under the pre-ASCE 7–16 loading scheme (Figure 7 black dashed curve). This is important because it suggests that the changes to the FBC in response to the ASCE 7–16 load increases are a conservative (more than sufficient) response. This conclusion is clearly couched within the compound uncertainties and simplifications in the FPHLM, and inherent in any wind hazard risk model.

Finally, the influence of the change in component capacities on individual component vulnerability is displayed in Figures 9, 10 for the strong model and new strong model roof sheathing damage under ASCE 7–10 and ASCE 7–16 respectively. Under both loading schemes, the roof sheathing in the new strong model is less vulnerable than the strong model as expected. Analogous to the conclusion in the previous paragraph, comparing Figure 6 (black dashed) to Figure 10 (red solid) shows that the updates

to the FBC more than compensate for the increased loading in ASCE 7–16 at the component level.

6 Conclusion and future work

The process of integrating ASCE 7–16 wind-load provisions into the FPHLM requires an understanding of the mechanical principles at work, engineering judgment, and iterative design based on analysis of previous versions. This comparative study demonstrates that the structural upgrades required to resist new uplift loads have a more significant impact on the vulnerability of the system than the new loads. The new model projections cannot be directly validated with field observations or insurance claims data, as no design-level events have impacted Florida since the enforcement of the FBC seventh Ed. The opportunity to validate this work will be pursued when nature provides. Earlier studies validating the FPHLM with insurance claims data were discussed in [Section 1](#).

Future developments involve implementing the changes presented in this paper into more structural models in the FPHLM. Within the single family residential model, the new loading scheme will need to be developed for the hip roof, a more complex geometry than the gable roof. New strong models will need to be developed for the masonry block models. Beyond the single family residential model, both the loading-side and capacity-side changes resulting from the ASCE 7–16 wind load provisions will be explored in the manufactured housing model, the low-rise commercial residential model, and the mid-/high-rise building model.

Data availability statement

The original contributions presented in the study are included in the article/supplementary material, further inquiries can be directed to the corresponding author.

References

- Abdelhady, A. U., Spence, S. M. J., and McCormick, J. (2022). Risk and fragility assessment of residential wooden buildings subject to hurricane winds. *Struct. Saf.* 94, 102137. doi:10.1016/j.strusafe.2021.102137
- American Society of Civil Engineers (2017). *Minimum design loads and associated criteria for buildings and other structures*. Virginia, United States: American Society of Civil Engineers. ASCE/SEI 7-16. doi:10.1061/9780784414248
- American Society of Civil Engineers (2013). *Minimum design loads for buildings and other structures*. Virginia, United States: American Society of Civil Engineers. ASCE/SEI 7-10. doi:10.1061/9780784412916
- Baheru, T. (2014). *Development of test-based wind-driven rain intrusion model for hurricane-induced building interior and contents damage*. Miami: Florida International University. dissertation.
- Berke, P., Larsen, T., and Ruch, C. (1984). A computer system for hurricane hazard assessment. *Comput. Environ. Urban Syst.* 9 (4), 259–269. doi:10.1016/0198-9715(84)90026-7
- Building a Safer Florida (2020a). Changes to wind loads in the 7th Edition. Florida Building Code, Building and Residential – Impacts from ASCE 7-16.

Author contributions

All authors listed have made a substantial, direct, and intellectual contribution to the work and approved it for publication.

Funding

This work is supported by Florida Office of Insurance Regulation (FOIR).

Acknowledgments

The authors wish to recognize the support of numerous FPHLM team members not directly involved in the production of this paper. The opinions, results, discussion, and conclusions are not necessarily those of the FOIR.

Conflict of interest

The authors declare that the research was conducted in the absence of any commercial or financial relationships that could be construed as a potential conflict of interest.

Publisher's note

All claims expressed in this article are solely those of the authors and do not necessarily represent those of their affiliated organizations, or those of the publisher, the editors and the reviewers. Any product that may be evaluated in this article, or claim that may be made by its manufacturer, is not guaranteed or endorsed by the publisher.

Available at: https://www.floridabuilding.org/fbc/Links_to_Code_Resources.html (Accessed July 1, 2022).

Building a Safer Florida (2020b). Florida building code – building, residential and existing building. Significant changes to roofing requirements in the 7th Edition. Available at: https://www.floridabuilding.org/fbc/Links_to_Code_Resources.html (Accessed July 1, 2022).

Chock, G., Ghosh, S. K., O'Rourke, M., and Stafford, T. E. (2018). *Significant changes to the minimum design load provisions of ASCE 7-16*. Virginia: American Society of Civil Engineers.

Cope, A. (2004). *Predicting the vulnerability of typical residential buildings to hurricane damage*. Gainesville (FL): University of Florida. dissertation.

Fema-Hazus (2006). *HAZUS-MH-MR3, multi-hazard loss estimation methodology hurricane model technical manual*. Washington D.C: Dept. Of Homeland Security, Federal Emergency Management Agency, Mitigation Division.

Florida Building Commission (2020). *Changes to the Florida building code*. Available at: https://www.floridabuilding.org/fbc/Links_to_Code_Resources.html (Accessed July 1, 2022).

- Florida International University (2021). Florida public hurricane loss model 8.1. Available at: <https://www.sbafla.com/methodology/ModelerSubmissions/CurrentYearHurricaneModelSubmissions.aspx> (Accessed July 1, 2022).
- Friedman, D. (1975). *Computer simulation in natural hazard assessment. Technical Report*. Boulder, (CO): University of Colorado.
- Hamid, S., Kibria, B. M. G., Gulati, S., Powell, M., Annane, B., Cocke, S., et al. (2010). Predicting losses of residential structures in the state of Florida by the public hurricane loss evaluation model. *Stat. Methodol.* 7, 552–573. doi:10.1016/j.stamet.2010.02.004
- Hamid, S. S., Pinelli, J.-P., Chen, S., and Gurley, K. (2011). Catastrophe model-based assessment of hurricane risk and estimates of potential insured losses for the state of Florida. *Nat. Hazards Rev.* 12, 171–176. doi:10.1061/(ASCE)NH.1527-6996.0000050
- International Code Council (2017). Florida building code, residential. Available at: <https://codes.iccsafe.org/content/FRC2017> (Accessed July 1, 2022). 6th Edition
- International Code Council (2020). Florida building code, residential. Available at: <https://codes.iccsafe.org/content/FLRC2020P1> (Accessed July 1, 2022). 7th Edition
- Ji, X., Huang, G., Wu, F., and Lu, Z. (2020). Wind-induced hazard assessment for low-rise building envelope considering potential openings. *J. Struct. Eng. (N. Y. N. Y.)* 146. doi:10.1061/(ASCE)ST.1943-541X.0002553
- Johnson, T., Pinelli, J.-P., Baheru, T., Chowdhury, A. G., Weekes, J., and Gurley, K. (2018). Simulation of rain penetration and associated damage in buildings within a hurricane vulnerability model. *Nat. Hazards Rev.* 19. doi:10.1061/(ASCE)NH.1527-6996.0000288
- Lin, S., Chuang, W., Xu, L., El-Tawil, S., Spence, S. M. J., Kamat, V. R., et al. (2019). *Framework for modeling interdependent effects in natural disasters: Application to wind engineering*. Virginia, United States: ASCE. doi:10.1061/(ASCE)ST.1943-541X.0002310
- Nofal, O. M., van de Lindt, J. W., Do, T. Q., Yan, G., Hamideh, S., Cox, D. T., et al. (2021). *Methodology for regional multihazard hurricane damage and risk assessment*. Virginia, United States: ASCE. doi:10.1061/(ASCE)ST.1943-541X.0003144
- Pinelli, J.-P., Gurley, K. R., Subramanian, C. S., Hamid, S. S., and Pita, G. L. (2008). Validation of a probabilistic model for hurricane insurance loss projections in Florida. *Reliab. Eng. Syst. Saf.* 93, 1896–1905. doi:10.1016/j.ress.2008.03.017
- Pita, G., Pinelli, J.-P., Cocke, S., Gurley, K., Mitrani-Reiser, J., Weekes, J., et al. (2012). Assessment of hurricane-induced internal damage to low-rise buildings in the Florida Public Hurricane Loss Model. *J. Wind Eng. Industrial Aerodynamics* 104–106, 76–87. doi:10.1016/j.jweia.2012.03.023
- Pita, G., Pinelli, J.-P., Gurley, K., and Mitrani-Reiser, J. (2014). *State of the art of hurricane vulnerability estimation methods: A review*. Virginia, United States: ASCE, 0000153. doi:10.1061/(ASCE)NH.1527-6996.0000153
- Prevatt, D. O., Hill, K. M., Datin, P. L., and Kopp, G. A. (2009). Revisiting wind uplift testing of wood roof sheathing – interpretation of static and dynamic test results. Proceedings of the Hurricane Hugo 20th Anniversary Symposium on Building Safer Communities—Improving Disaster Resilience, Charleston, South Carolina, October 22 – 23, 2009.
- Ruch, C. (1984). *Hurricane vulnerability analysis for aransas, kenedy, kleberg, nueces, refugio, and san patricio counties*. Austin, TX: Texas A&M University for the Governor's Division of Emergency Management.
- Sciaudone, J., Feuerborn, D., Rao, G., and Daneshvaran, S. (1997). *Development of objective wind damage functions to predict wind damage to low-rise structures*. Baltimore, Maryland: 8th U.S. National Conf. on Wind Engineering.
- Scott, D. (2018). ASCE 7-16 wind load provisions – how they affect the practicing engineer. *Struct. Mag.*, 12–14.
- Silva de Abreu, R. V., Pinelli, J.-P., Raji, F., and Zisis, I. (2020). Testing and modeling of hurricane wind-driven rain water ingress, propagation, and subsequent interior damage in residential buildings. *J. Wind Eng. Industrial Aerodynamics* 207, 104427. doi:10.1016/j.jweia.2020.104427
- Skulteti, M. J., Bender, D. A., Winistorfer, S. G., and Pollock, D. G. (1997). Withdrawal strength of ring-shank nails embedded in southern pine lumber. *Trans. ASAE* 40 (2), 451–456. doi:10.13031/2013.21272
- Southwest Florida Regional Planning Council (Swfrpc) (1982). *Southwest Florida hurricane loss study*. United states: SWFRPC.
- Sparks, P., and Bhinderwala, S. (1994). “Relationship between residential insurance losses and wind conditions in hurricane Andrew,” in *Hurricanes of 1992: Lessons learned and implications for the future*. Editors R. Cook and M. Sotani (Virginia, United States: ASCE), 111–124.
- Strong-Tie Company, S (2021). Wood construction connectors 2021-2023. Available at: <https://www.strongtie.com/resources/literature/wood-construction-connectors-catalog> (Accessed July 1, 2022).
- Torkian, B. B., Pinelli, J.-P., Gurley, K., and Hamid, S. (2014). *Cost-and-benefit evaluation of windstorm damage mitigation techniques in Florida*. Virginia, United States: ASCE, 0000122. doi:10.1061/(ASCE)NH.1527-6996.0000122
- WJHG News (2017). Florida's highest point is right in our own backyard. Available at: <https://www.wjhg.com/content/news/Floridas-highest-point-is-right-in-our-own-backyard-459451853.html> (Accessed July 1, 2022).